Catalysis Today 429 (2024) 114470

Contents lists available at ScienceDirect

Catalysis Today

journal homepage: www.elsevier.com/locate/cattod

# On the selective transformation of ethanol over Mg- and/or La-containing mixed oxides catalysts

D. Ballesteros Plata [a], G. Balestra [b,c], J.A. Cecilia [a,*], I. Barroso Martín [a], A. Infantes-Molina [a], T. Tabanelli [c], F. Cavani [c], J.M. López Nieto [b,*], M. Montaña [d], E. Rodríguez Castellón [a]

[a] Departamento de Química Inorgánica, Facultad de Ciencias, Universidad de Málaga, Campus de Teatinos, 29071 Málaga, Spain
[b] Instituto de Tecnología Química, Universitat Politècnica de València-Consejo Superior de Investigaciones Científicas, Avenida de los Naranjos s/n, 46022 Valencia, Spain
[c] Dipartimento di Chimica Industriale "Toso Montanari", Universitá di Bologna, Viale del Risorgimento 4, Bologna, Italy
[d] Departamento de Tecnología Química, Energética y Mecánica, Escuela Superior de Ciencias Experimentales y Tecnología, Universidad Rey Juan Carlos, calle Tulipán s/n, Madrid, Spain

ARTICLE INFO

*Keywords:*
Ethanol
Ethylene
Acetaldehyde
Butanol
Gas-phase
Heterogenous catalyst

ABSTRACT

MgO-$La_2O_3$ catalysts with different Mg/La molar ratio were synthesized by a precipitation method and a subsequent calcination and then characterized by x-ray diffraction, $N_2$ adsorption-desorption isotherms (at −196 °C), $CO_2$- and $NH_3$-thermoprogrammed desorption and x-ray photoelectronic spectroscopy. The coexistence of acid and basic sites promoted the selective transformation of ethanol into valuable products. Thus, MgO catalyst promoted the Guerbet reaction obtaining *n*-butanol as product while the incorporation of $La_2O_3$ in the catalytic system improved the ethanol conversion notably, obtaining ethylene as the main product due to a dehydration reaction. The highest ethylene yield was obtained for the catalyst with a Mg/La molar ratio of 1.

## 1. Introduction

The adverse effects of the combustion of fossil fuels together with their progressive depletion have given rise to the search and development of alternative energy sources, which must be highly available and environmentally benign [1]. In this sense, biomass is a very interesting source since it is abundant in the Earth and it is an alternative from which energy can be obtained, but also chemical products, which are currently obtained from fossil fuels. Biomass is a highly available resource; however, its selection must be detailed since inappropriate use can interfere with the food chain, causing speculation problems and social imbalances. Under these premises, biomass from agricultural waste could be a potentially sustainable source of biomass. These wastes are generally composed of lignocellulosic biomass, which contains lignin, cellulose and hemicellulose. The chemical composition of each fraction is variable depending on the variety of plants. The interest in the valorization of this waste has given rise to the implantation of sugar platforms where this type of biomass is transformed into high added value products [2]. Among the chemicals obtained in the sugar platform, ethanol is the most abundant product with an annual production of around 100 billion of liters per year [3]. This ethanol is obtained by fermentation of the sugars with the yeast *Saccharomyces cerevisiae* [4–6]. Nowadays, bioethanol has been widely employed independently or mixed with traditional fuels. However, one of the main drawbacks of using ethanol as fuel is related to its low vapor pressure and $H_2O$ adsorption capacity. This means separation problems in storage tanks as well as high corrosiveness in engines. Nowadays, bio-ethanol can be used as an additive in engines without modifications at small levels. However, the use of high percentage ethanol mixtures as fuel requires engines modifications. This limitation can be minimized with the use of alcohols with larger chain, which display better properties for their application as fuel [7].

Bio-ethanol can also be utilized to obtain other valuable products. Among them, ethylene is the dehydration reaction product of ethanol. Ethylene is considered a key feedstock for the chemical industry because it can be converted into a wide range of products such as ethylene oxide, ethylbenzene, 1,2-dichloroethane, polyethylene resin, ethylene glycol, vinyl chloride resin, acetic acid, styrene, and alpha olefin, among others [8]. Thus, global ethylene consumption was ca. 200 MMT by 2020, with production capacities of 185 MMT in 2019 [9]. Traditionally, ethylene has been synthesized by steam cracking; however, this process requires a high-energy demand. Considering the high interest of ethylene for the

* Corresponding authors.
*E-mail addresses:* jacecilia@uma.es (J.A. Cecilia), jmlopez@itq.upv.es (J.M. López Nieto).

https://doi.org/10.1016/j.cattod.2023.114470
Received 20 July 2023; Received in revised form 10 November 2023; Accepted 21 November 2023
Available online 24 November 2023

synthesis of other chemical products, it is necessary to research and develop alternative methodologies for the synthesis of this product.

The dehydration reaction of alcohols takes place through solid acid catalysts [10–12]. Previous authors have reported that the reaction occurs through an intramolecular mechanism where the acid sites of the catalyst attack the labile hydrogen of the hydroxyl group followed by the release of $H_2O$. Then, the primary carbocation formed is attacked by the conjugated base of the catalyst, forming ethylene and regenerating the catalyst. In addition, the intermolecular dehydration is possible, forming diethyl ether, which is exothermic, so both reactions can compete between them [13,14] although some authors have pointed out that the use of high temperature promotes the formation of ethylene while the use of low temperature favors the formation of diethyl ether [15,16].

$$C_2H_5OH \rightarrow C_2H_4 + H_2O \qquad \Delta H^{\circ}_{298K} = +44.9 kJ/mol$$

$$C_2H_5OH \rightarrow (C_2H_5)_2O + H_2O \qquad \Delta H^{\circ}_{298K} = -25.1 kJ/mol$$

Once ethylene is formed, this compound can evolve towards other undesired products due to cracking, oligomerization, cyclization or aromatization reactions, which are accompanied by the formation of coke and, consequently, the deactivation of the catalysts [17].

The first studies for the ethanol dehydration were performed with $Al_2O_3$ as acid catalyst [18]. More recently, many studies have been carried out with zeolites because it is possible to work with zeolites with narrow pore size distribution, modulable acidity and it is possible to incorporate some promoters to improve both conversion and yields [19–21]. In the same way, other acid catalysts tested in ethanol dehydration are silicoaluminophosphates (SAPO) [22] or heteropolyacids (HPAs) [23,24]. In the same way, the use of some dopants such as P, Ga, Zr, W or La among other has been incorporated to improve the yield towards ethylene [13,25,26].

In an opposite trend, the ethanol transformation over oxide catalysts with basic characteristics led to the formation of important chemicals such as 1-butanol (by Guerbet reaction) and 1,3-butadiene (by Lebedev reaction [27]), as occurs over MgO catalysts [27,28]. However, in the presence of catalysts with acid-basic sites, as in Mg-Al oxide [29], it has been observed that these catalysts are active in the dehydration reaction, yielding ethylene (because of the presence of acid sites) and dehydrogenation reactions, yielding acetaldehyde (catalyzed by medium-strength basic sites), which, in turn, can lead the selective transformation of ethylene.

Regarding lanthanum-based catalysts, Garbarino et al. have reported that the impregnation of $La_2O_3$ into $Al_2O_3$ improves the mechanical strength [30,31] and stabilizes the structure, avoiding its sintering [30,32]. These authors obtained a large amount of ethylene while the diethyl ether formed is converted to ethylene and $H_2O$, which is promoted by the presence of Lewis acid sites [30]. In addition, it has been observed how the presence of $La_2O_3$ also limits the formation of coke so that the catalysts can be stable for a longer reaction time [30,33]. Other authors have reported that the presence of lanthanum generates acid sites, which could be involved in the ethanol dehydration, due to the hydrolysis of the hydrated cations and the coverage of the active centers [34,35].

Taking into account the good role played by lanthanum species in ethanol dehydration, in this work $MgO/La_2O_3$ catalysts were prepared, obtained from their respective hydroxides under controlled pH to improve the dispersion of these species. In order to evaluate the activity of $La_2O_3$ and MgO in the catalytic behavior, several catalysts with different Mg/La molar ratios were prepared and these catalysts were tested in the potential dehydration or condensation of ethanol.

## 2. Experimental

### 2.1. Materials

Reagents and standards were of analytical grade, in particular: absolute ethanol (Scharlab); $Mg(CH_3COO)_2{\cdot}4\ H_2O$ (%), $C_2O_4H_2{\cdot}2\ H_2O$ solution (99%), $La(NO_3)_3{\cdot}6\ H_2O$ and $Mg(NO_3)_2{\cdot}6\ H_2O$ were obtained from Sigma Aldrich and used as received.

### 2.2. Synthesis of the catalysts

The synthesis of $La_2O_3$ catalyst was carried out by the dissolution of 0.05 moles of La salt, i.e., $La(NO_3)_3{\cdot}6\ H_2O$, in 500 mL of $H_2O$. After that, the pH of the solution was increased by adding a mixture solution of 0.1 M NaOH and 0.25 M $Na_2CO_3$ dropwise under stirring until a pH of 10 was reached, obtaining a gel. This gel was stirred for 30 min and then filtered and washed to remove $Na^+$ cations. In the next step, the solid was dried at 80 °C overnight and finally calcined at 600 °C for 3 h, employing a heating ramp of 2 °C $min^{-1}$.

The synthesis of $La_2O_3$-MgO catalysts with different Mg/La molar ratios was carried out by following the same procedure as for pure $La_2O_3$ sample, but adding different molar amounts of Mg salt ($Mg(NO_3)_2{\cdot}6\ H_2O$) during the solution of 0.05 moles of La salt in 500 mL of water, depending on the Mg/La ratio desired. The samples were referred to as Mg/La= x, where x stands for the Mg/La molar ratio employed in the synthesis.

Magnesium oxide was synthesized by a precipitation method [36]. A solution containing magnesium acetate (i.e., $Mg(CH_3COO)_2{\bullet}4\ H_2O$) and oxalic acid (i.e., $C_2O_4H_2{\cdot}2\ H_2O$) was conducted to pH 5 through a 1.3 M $NH_4OH$ solution. The resulting magnesium oxalate β-$MgC_2O_4$ precipitate was separated by filtration, washed, and dried at 80 °C overnight and calcined at 600 °C for 3 h, with a heating ramp of 2 °C $min^{-1}$, obtaining the corresponding magnesium oxide MgO.

### 2.3. Characterization techniques

Samples were characterized by adsorption-desorption of $N_2$ at − 196 °C to determine the specific surface area and the porosity through a Micromeritics ASAP 2420 apparatus. Prior to the analysis, samples were degassed at 150 °C for 20 h.

Calcined and spent catalysts were analyzed by X-ray powder diffraction (XRD) on a PAN analytical X'Pert Pro automated diffractometer. The analysis was done in the high angle region, between 5 and 80° in 2θ with a step size of 0.0167° (2θ) and an equivalent counting time of ~60 s/step, using a Ge (111) primary monochromator, a monochromatic Cu Kα radiation (λ = 1.5406 Å) and an X´Celerator detector.

The particle size distribution was obtained with a High-Resolution Transmission Electron Microscopy (HRTEM) TALOS F200x instrument. The device also operates in STEM mode (Scanning Transmission Electron Microscopy), with a HAADF detector, at 200 kV and 200 nA. The microanalysis was carried out with an EDX Super-X system provided with 4 X-ray detectors and an X-FEG beam.

The surface composition of calcined and spent catalysts was analyzed by X-ray photoelectron spectroscopy (XPS) using a Physical Electronics PHI 5701 apparatus. A non-monochromatic Mg-$K_\alpha$ radiation (720 μm, 300 W, 15 kV, 1253.6 eV) and a multi-channel detector were used. Samples were analyzed in a constant pass energy mode at 29.35 eV, and the adventitious carbon (284.8 eV) in C1*s* signal was used as reference charge. In order to remove the potential carbonatation of $La_2O_3$ and MgO, the samples were recalcined at 950 °C/6 h (5 °C $min^{-1}$). After calcination, the samples were immediately stored in a desiccator provided with drying agents, and quickly loaded into the XPS equipment. The La 3*d* core level spectrum could not be deconvoluted because the baseline cut the spectra. Therefore, the signal La $3d_{5/2}$ was studied.

The basicity of the samples was determined by thermo-programmed desorption of $CO_2$ ($CO_2$-TPD), and the acidity was determined by thermo-programmed desorption of $NH_3$ ($NH_3$-TPD). In both cases, the desorption was measured between 60 and 700 °, using an AutoChem 2920 apparatus equipped with a TCD detector.

**Table 1**
Textural and Surface characteristics of calcined catalysts.

| Catalyst | $S_{BET}$ ($m^2\ g^{-1}$) | $V_p$ ($cm^3\ g^{-1}$) | C 1*s* | O 1*s* | Mg 2*p* | La 3*d* | Surface Mg/La ratio | Basicity ($\mu mol_{CO2}\ g^{-1}$) | Acidity ($\mu mol_{NH3}\ g^{-1}$) |
|---|---|---|---|---|---|---|---|---|---|
| $La_2O_3$ | 6 | 0.012 | 22.2 | 48.0 | - | 27.3 | - | 56 | 9.0 |
| Mg/La= 1 | 31 | 0.050 | 17.2 | 46.4 | 24.0 | 10.2 | 2.3 | 289 | 9.0 |
| Mg/La= 2 | 16 | 0.046 | 15.2 | 47.7 | 27.6 | 7.3 | 3.8 | 177 | 11 |
| Mg/La= 3 | 18 | 0.054 | 18.1 | 46.9 | 25.1 | 5.0 | 5.0 | 184 | 10 |
| Mg/La= 4 | 23 | 0.061 | 17.6 | 46.3 | 29.0 | 5.5 | 5.3 | 295 | 13 |
| MgO | 91 | 0.368 | 14.4 | 48.0 | 37.6 | - | - | 648 | - |

### 2.4. Catalytic tests

The catalytic experiments were performed using a conventional system with a fixed bed quartz-reactor at atmospheric pressure. The feed composition was $EtOH/N_2 = 5/95$ molar ratio. All the reactions were carried out by keeping a Weight Hourly Space Velocity of 0.30 $g_{EtOH}\ g_{cat}^{-1}\ h^{-1}$. The reaction temperature was varied in the range 350–400 °C. Each reaction has been performed with a total time on stream of 3 h.

The deactivation rate during the first 1.5 h of catalytic tests was very low, fore some catalysts a change in the catalytic behavior after 1.5 h of time on stream was observed. Therefore, the values of ethanol conversion (X,%) and the selectivity to main reaction products (Si, %) were calculated considering the average of 3 values obtained int the range of time on stream between 0.7 and 1.5 h.

In this sense, in a typical reaction test, all the catalysts were pretreated at 600 °C for 2 h under Air flow before of being charged into the reactor to be pre-heated at 120 °C. At this temperature, the vaporized ethanol was fed and analyzed with an on-line GC in order to evaluate the exact starting concentration of the reagent. After that, the temperature of the furnace was set to the desired reaction temperature and when reached, the reaction started. For each reaction, fresh new catalysts were loaded inside the reactor.

The reaction products were monitored by on-line gas chromatography (Agilent 7890 A) equipped with two capillary columns: an HP-FFAP Polyethylene glycol (50 m x 320 μm x 0.5 μm) connected to a FID detector and a Rt-U-Bond (30 m x 530 μm x 20 μm) column connected to a TCD detector. The by-products were analyzed by GC-MS (Agilent 6890 N system, equipped with a capillary HP-5MS (5%Phenyl Methyl Siloxane) (30 m x 250 μm x 0.25 μm) and coupled with Agilent 5973 N mass detector). Comprehensive explanation of compounds quantifications can be found in the Table S1, supporting information.

## 3. Results and discussion

### 3.1. Characterization of the calcined catalysts

The $N_2$ adsorption-desorption isotherms of the catalysts (Fig. S1, supporting information) suggest that, except in the case of pure MgO, the catalysts present a type II isotherm according to the IUPAC classification [37], which corresponds to macroporous solids where this macroporosity must be assigned to the voids between adjacent particles. In the case of the MgO sample, its isotherm resembles a type IV, which is

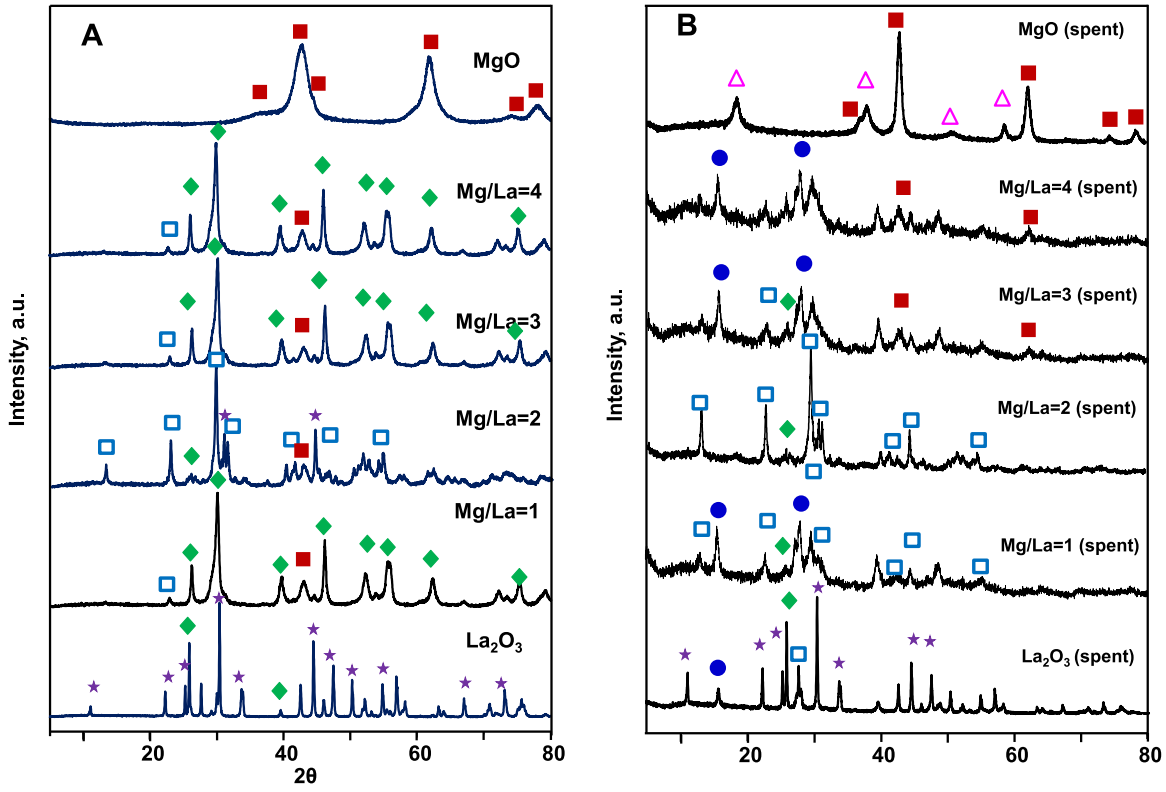


**Fig. 1.** XRD patterns of the catalysts before (A) and after catalytic tests (B). Symbols: MgO periclase, 01–074–1225 (■); $La_2O_3$ hexagonal, 01–083–1344 (♦); monoclinic $La_2O_2CO_3$, 00–025–0422 (□); orthorhombic $LaO_2CO_3$, 00–022–1127 (❋); $Mg(OH)_2$, 00–007–0239 (△); $La(OH)_3$, 00–036–1481 (●).

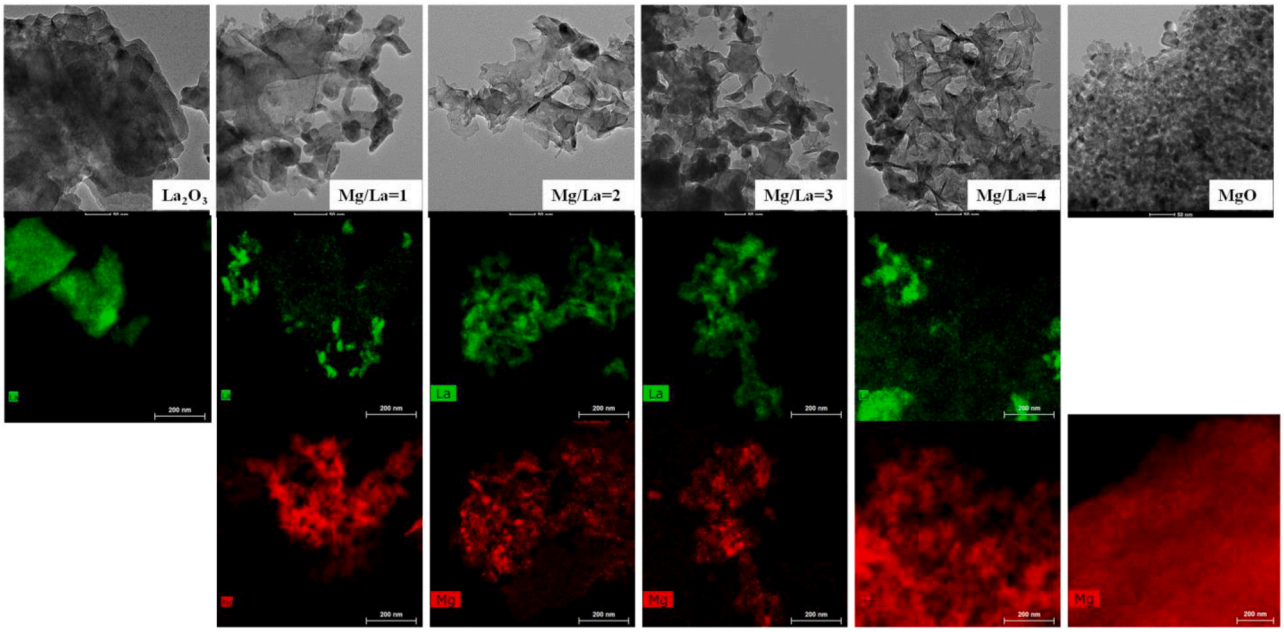


**Fig. 2.** HRTEM and STEM-EDX micrographs of the calcined samples. Characteristics of catalysts in Table 1.

typical of mesoporous materials [37]. Thus, the higher amount of $N_2$-adsorbed at high relative pressure, i.e., the higher microporosity, is more pronounced in the case of MgO/$La_2O_3$ catalysts, while the pure MgO and $La_2O_3$ display more limited microporosity.

Regarding to the analysis of the specific surface area, determined by the BET equation [38], MgO-$La_2O_3$ samples show similar surface areas (Table 1), between 15 and 31 $m^2\ g^{-1}$, while the pristine $La_2O_3$ sample displays the poorest surface area, only 6 $m^2\ g^{-1}$. On the opposite side, the MgO sample reported the highest $S_{BET}$ value (91 $m^2\ g^{-1}$).

The study of the pore volume (Table 1) shows a defined trend. The $La_2O_3$ sample shows the lowest pore volume value (0.012 $cm^3\ g^{-1}$), whereas the incorporation of MgO in the catalytic system increases the pore volume, attaining the highest value for the pure MgO sample (0.368 $cm^3\ g^{-1}$).

The study of the crystalline phase was carried out by XRD (Fig. 1). From these data, it can be observed how the $La_2O_3$ sample displays narrower peaks in comparison to the other catalysts. This implies that this catalyst has a higher crystallinity. This result is related to the analysis of the textural properties where the presence of larger crystals implies lower porosity. The identification of the diffraction peaks of the $La_2O_3$ sample indicates the coexistence of two phases: i) $La_2O_3$, with diffraction peaks at 2θ (°)= 26.14, 39.68, 46.12, 52.46, 55.60, 62.44 and 75.41 (Ref. code: 1–083–1344); and, ii) $La_2O_2CO_3$, with diffraction peaks at 2θ (°)= 11.08, 22.27, 25.83, 27.61, 30.36, 33.67, 42.53, 44.42, 47.44, 54.75, 58.18, 67.00, 83.98 and 86.09 (PDF number: 00–022–1127). These results suggest that $La_2O_3$ is highly prone to suffer carbonation processes. In addition, the carbonation degree of $La_2O_3$ as well as the crystallinity species decreases according to Mg-species are incorporated into the catalysts, although it was observed the presence of monoclinic $La_2O_2CO_3$ (PDF number: 00–025–0422). In addition, it is noteworthy the absence of carbonate crystals in the MgO sample. This suggests that the MgO-crystals are less prone to carbonate. Only for the sample with the composition of Mg/La = 2, the presence of lanthanum oxyhydroxide, LaOOH (PDF number: 01–077–2349), with diffraction peaks at 2θ (°)= 31.09, 31.59 and 40.88, cannot be ruled out. Moreover, the progressive addition of Mg-species leads to the presence of broad diffraction peaks located at 2θ (°) = 36.89, 42.86, 62.22 and 78.51, which are assigned to the MgO periclase (PDF number: 01–079–0612).

**Table 2**
C 1*s*, O 1*s*, La 3$d_{5/2}$ and Mg 2*p* signals for calcined samples.

| Sample | Signal | C 1*s* | | O 1*s* | | La 3$d_{5/2}$ | | Mg 2*p* |
|---|---|---|---|---|---|---|---|---|
| **$La_2O_3$** | *BE (eV)* | 284.8 | 289.5 | 528.8 | 531.4 | 833.7 | | - |
| | ***Species*** | **C-C** | **$CO_3^{2-}$** | **$La_2O_3$** | **$CO_3^{2-}$** | **$La_2O_3$ /$La_2(CO_3)_3$** | | - |
| | *AC (%)* | 19.1 | 3.0 | 24.5 | 23.5 | 1.4 | 1.2 | - |
| **Mg/La= 1** | *BE (eV)* | 284.8 | 289.5 | 529.3 | 531.5 | 833.7 | | 49.4 |
| | ***Species*** | **C-C** | **$CO_3^{2-}$** | **Oxides** | **$CO_3^{2-}$** | **$La_2O_3$/$La_2(CO_3)_3$** | | **MgO** |
| | *AC (%)* | 15.5 | 1.6 | 28.0 | 18.4 | 1.2 | 1.0 | 24.0 |
| **Mg/La= 2** | *BE (eV)* | 284.8 | 289.4 | 529.4 | 531.5 | 833.8 | | 49.3 |
| | ***Species*** | **C-C** | **$CO_3^{2-}$** | **Oxides** | **$CO_3^{2-}$** | **$La_2O_3$ /$La_2(CO_3)_3$** | | **MgO** |
| | *AC (%)* | 13.6 | 1.5 | 29.0 | 18.7 | 1.2 | 1.1 | 27.6 |
| **Mg/La= 3** | *BE (eV)* | 284.8 | 289.5 | 529.6 | 531.6 | 834.1 | 837.9 | 49.5 |
| | ***Species*** | **C-C** | **$CO_3^{2-}$** | **Oxides** | **$CO_3^{2-}$** | **$La_2O_3$ /$La_2(CO_3)_3$** | | **MgO** |
| | *AC (%)* | 16.9 | 1.2 | 25.1 | 21.8 | 2.6 | 2.3 | 25.1 |
| **Mg/La= 4** | *BE (eV)* | 284.8 | 289.6 | 529.7 | 531.8 | 834.1 | | 49.4 |
| | ***Species*** | **C-C** | **$CO_3^{2-}$** | **Oxides** | **$CO_3^{2-}$** | **$La_2O_3$ /$La_2(CO_3)_3$** | | **MgO** |
| | *AC (%)* | 16.1 | 1.4 | 30.0 | 16.2 | 0.9 | 0.8 | 29.0 |
| **MgO** | *BE (eV)* | 284.8 | 290.1 | 529.5 | 531.5 | - | - | 49.0 |
| | ***Species*** | **C-C** | **$CO_3^{2-}$** | **Oxides** | **$CO_3^{2-}$** | **-** | **-** | **MgO** |
| | *AC (%)* | 25.5 | 1.8 | 31.6 | 29.8 | - | - | 24.5 |

BE: binding energy; AC: atomic concentration percentage.

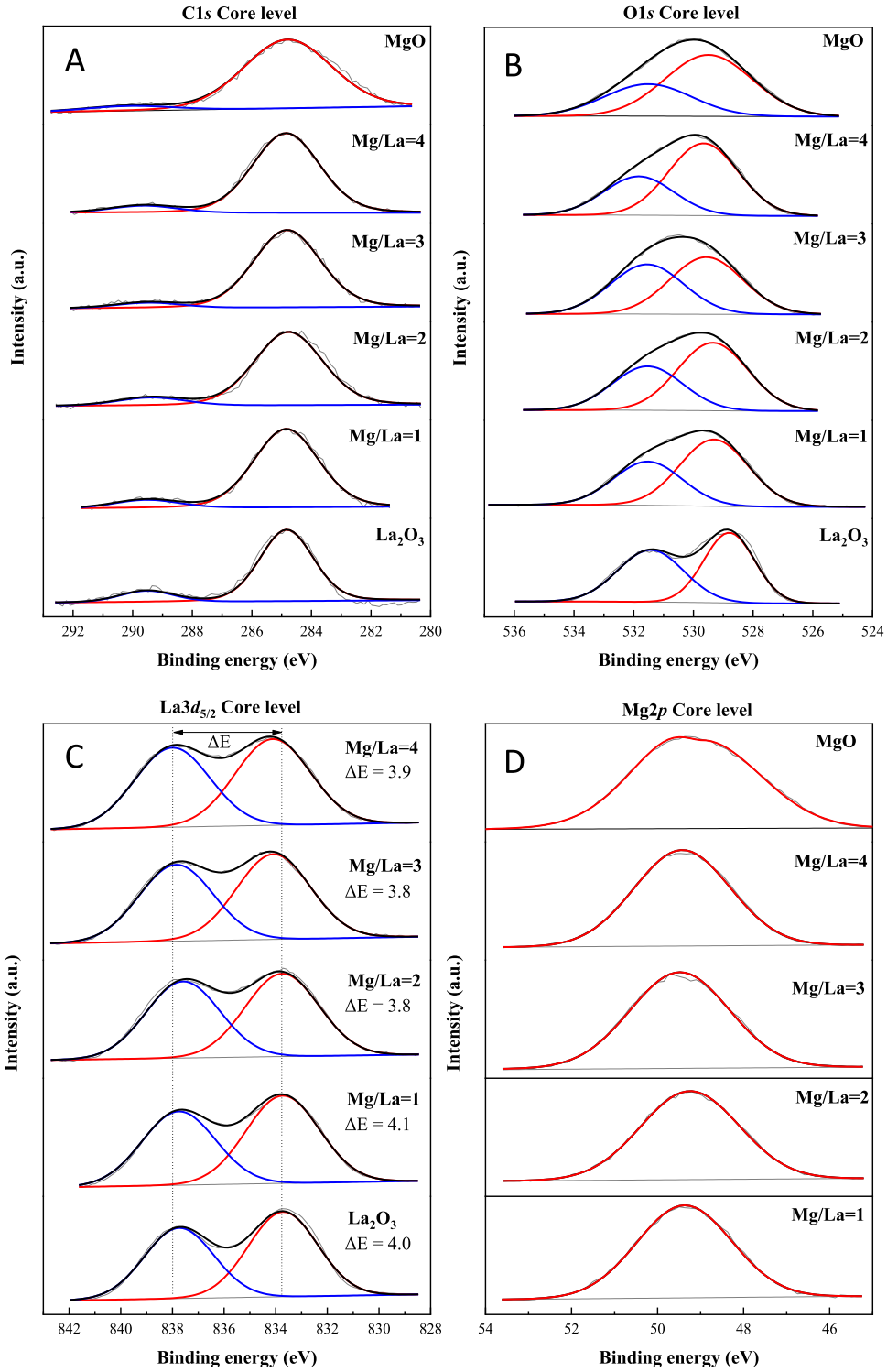


**Fig. 3. :** C 1*s* (A), O 1*s* (B), La $3d_{5/2}$ (A) and Mg 2*p* (B) core level spectra of calcined catalysts.

On the other hand, the presence of broader diffraction peaks suggests that MgO crystals are smaller than those obtained for $La_2O_3$. These data can be related to the increase in surface area when Mg-species are incorporated due to the presence of smaller particles generating more voids and consequently greater porosity, as indicated the study of the textural properties (Table 1). In addition, it is also noteworthy that absence of carbonate crystals in the MgO sample. This suggests that the MgO-crystals, which are also more dispersed due to their lower crystallinity, are less prone to carbonate.

The morphology of the catalysts was analyzed by HRTEM (Fig. 2). These micrographs show that the $La_2O_3$ sample displays bigger particles, which can be related to its lowest surface area. The incorporation of Mg-species in the form of MgO leads to a progressive decrease of the particle size such that MgO catalyst has a smaller crystal size. In this sense, the smaller particles in the MgO catalyst must be directly related to a higher specific surface area (Table 1). The EDX analysis of MgO-$La_2O_3$ samples shows how La- and Mg-species are agglomerated by zones. However, the formation of homogeneous $MgLa_2O_4$ were not observed by XRD despite

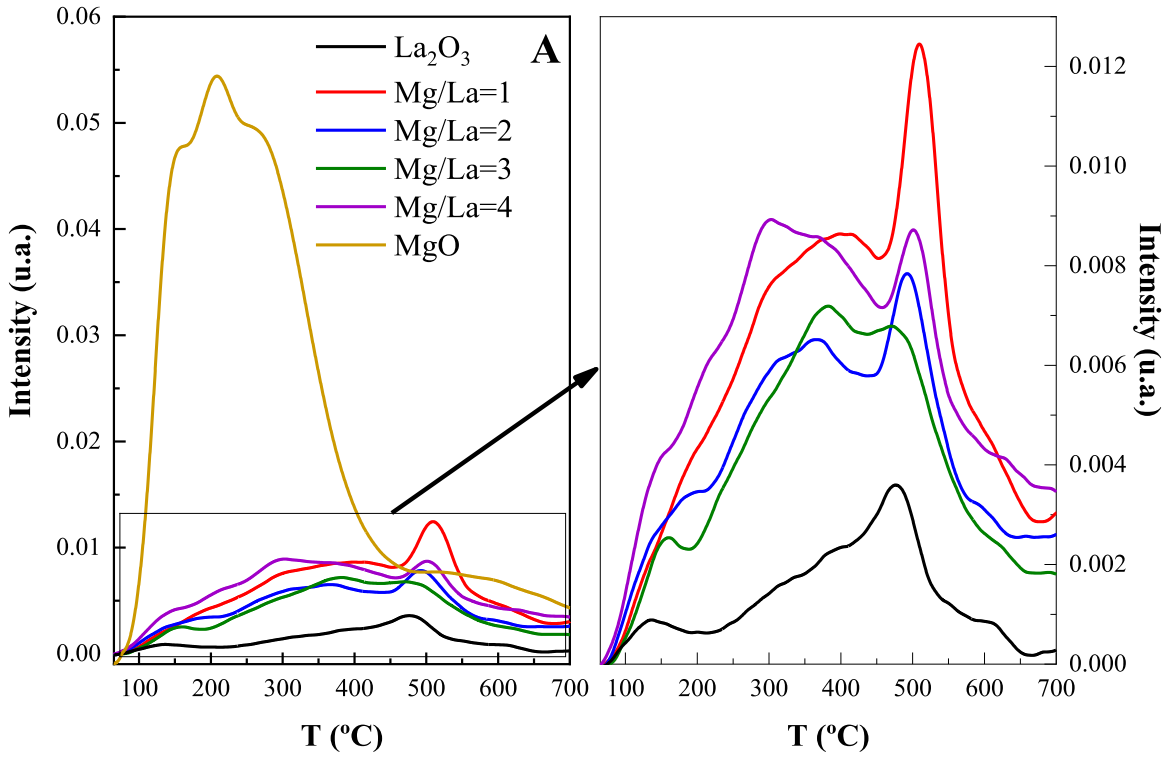


**Fig. 4.** $CO_2$-TPD desorption profiles of calcined catalysts.

calcining materials at 600 °C.

The surface atomic concentration of the catalyst is compiled in (Table 2). These data reveal how the Mg/La molar ratios on the surface of catalysts are higher than the theoretical Mg/La values in all MgO-$La_2O_3$ catalysts, so it is expected that Mg-species are more exposed in the surface of the catalyst in comparison to $La_2O_3$.

The detailed analysis of C1*s* core level spectra shows two contributions (Fig. 3A). The main contribution located at 284.8 eV (adventitious carbon) is used as reference to counteract the displacement of charge [39].

The low intensity contribution, located about 289.5 eV, is ascribed to the presence of carbonate species [39]. Thus, despite to the previous calcination treatment to remove the carbonate species, it has not been possible to avoid a partial recarbonation in the handling. In this sense, the analysis of the carbonate/adventitious carbon ratio reveals that the $La_2O_3$ catalyst is more prone to carbonation (0.16) than the rest of the catalysts. In the same way, the progressive incorporation of Mg-species diminishes the trend to the carbonatation since the carbonate/adventitious carbon ratio is only of 0.07.

The analysis of the O1*s* core level spectra also displays two contributions (Fig. 3B). The contribution located at the low binding energy region (529.3–529.7 eV) is assigned to the presence of oxides species in the form of MgO, $La_2O_3$ or MgO-$La_2O_3$ [39]. In the case of the contribution at the highest binding energy value (531.5–531.9 eV), this contribution is attributed to the presence of carbonate species [39], increasing the intensity of the contribution with the La content, which agrees with the study of the C 1 *s* core level spectra.

The analysis of the La $3d_{5/2}$ core level spectra show values at 833.7–834.1 eV (Fig. 3C). typical of La(III) as $La_2O_3$ or $La_2(CO_3)_3$. The analysis of the Mg 2*p* core level spectra display a unique contribution located at 49.0–49.6 eV, that is assigned to Mg-species in the form of oxide and/or carbonate (Fig. 3D) [39]. In addition, it is also noteworthy that the incorporation the presence of La-species in the catalyst causes a shift of the binding energy of the Mg-species at higher values. This shift is ascribed to the modification of the electronic density of the Mg-species by the presence of La-species [39].

The analysis of the acid and basic sites, which are involved in the reaction, was also carried out. The study of the basic sites by $CO_2$-TPD shows how the samples desorb $CO_2$ in a broad range of temperature, between 100 and 500 ºC (Table 1 and Fig. 4A). This figure shows how the $La_2O_3$ sample displays a maximum of $CO_2$-desorption about 480 °C while the MgO sample desorbs at lower temperature, suggesting that La-sites have stronger basicity than Mg-sites. These data are in agreement with the characterization results where it seems that $La_2O_3$ sites are more prone to suffer carbonation processes due to the stronger basicity in comparison to MgO. The analysis of the MgO-$La_2O_3$ catalysts displays two defined sections. The first one, at lower temperature, is assigned to weaker basic-sites, which are attributed to MgO-sites, while the signal located at higher temperature is assigned to stronger basic-sites due to the presence of $La_2O_3$. The quantification and the analysis of the density of basic sites (Table 1 and Table S2, supplementary information) reveals that the addition of Mg-species increases of the total amount as well as the density of basic sites due to the higher surface area shown for the catalysts with high Mg-content. Despite MgO sample displays a high number of basic sites, these sites are milder than those reported for La-based catalysts.

The quantification and the strength of the acid sites were analyzed by $NH_3$-TPD (Table 1 and Table S2 and Fig. S2, supporting information). The obtained data reveal that, as expected, the amount of acid sites is negligible in comparison to the basic ones, reaching a maximum value of only of 13 $\mu mol_{NH3}\ g^{-1}$ for Mg/La= 4 catalyst. The study of the density of acid sites reveals that the incorporation of Mg-species diminishes the amount of acid sites per surface unit.

### 3.2. Catalytic results

Several blank tests were performed by feeding ethanol into the reactor, in the absence of the catalytic bed, in the range of the desired temperatures (300 – 400 °C), and no EtOH conversion was detected along the temperature range evaluated.

Then, the catalytic activity of the pre-treated catalysts (at 600 °C/2 h as reported in experimental part) was tested. In all cases, the reactivity

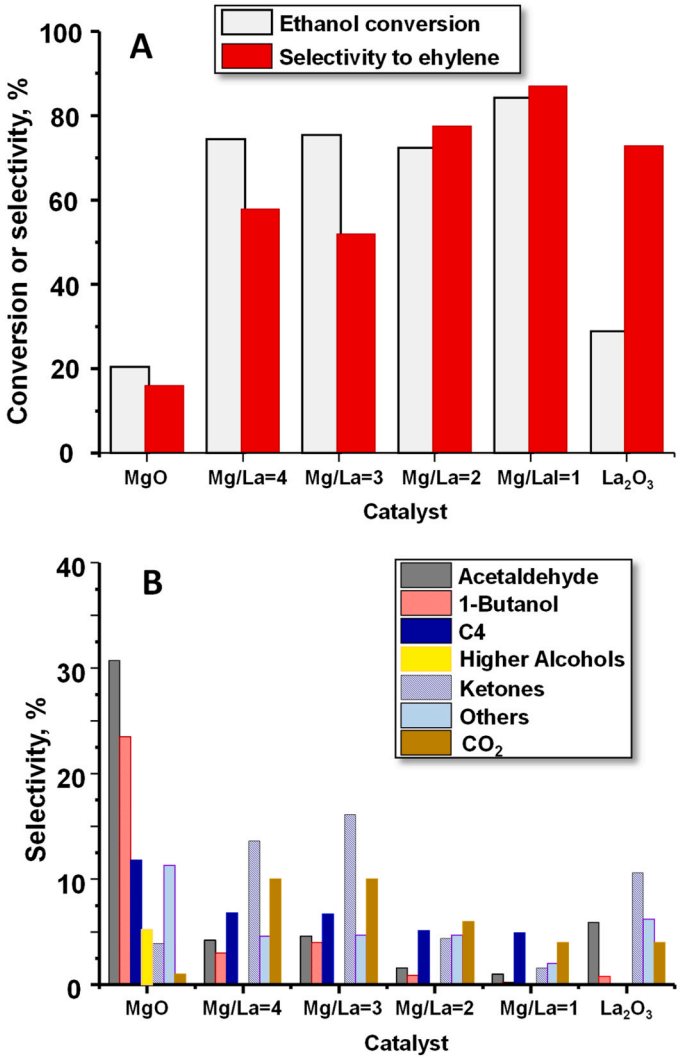


**Fig. 5.** Ethanol conversion and selectivity to ethylene (A) and selectivity to the rest of the reaction products (B) during the ethanol transformation over Mg- and or La-containing catalysts. Reaction conditions: EtOH 5% v/v in $N_2$; T = 400 °C; P = 1 atm; WHSV= 0.3 $g_{ETOH}$ $g_{CAT}^{-1}$ $h^{-1}$. **Higher alcohols**: 2-ethyl butanol, 1-hexanol, 2-ethyl butanol; **Ketones**: acetone, 2-pentanone; $C_4$: 1,3-butadiene, **Others**: ethyl ether, butyraldehyde, ethane.

tests were carried out at 400 °C, with a percentage of EtOH in the feed stream equal to 5 mol% in $N_2$ while keeping a weight hourly space velocity (WHSV) of 0.3 $g_{ETOH}$ $g_{CAT}^{-1}$ $h^{-1}$). The results, expressed in terms of conversion of EtOH and selectivity to ethylene (Fig. 5A), as well as the selectivity to the rest of the reaction products (Si, %) (Fig. 5B), are also summarized in Table 3.

MgO is a well-known heterogeneous catalyst for the Guerbet reaction, used many times as reference catalyst to study its mechanism [27,40,41]. Indeed, while performing the reaction over MgO, the Guerbet reaction product of ethanol, *n*-butanol, and the intermediate product (acetaldehyde), were observed as main products, with a selectivity as high as 23.5% and 30.7%, respectively and with an ethanol conversion of 20%.

Even 1,3-butadiene production was observed, with a selectivity of 12%. Its production could occur through a mechanism based on the aldolic condensation of acetaldehyde [42], or by considering crotyl alcohol and 3-buten-1-ol as the key intermediates of the Lebedev process for butadiene formation [27,28,41].

The presence of lanthanum in the catalytic system had many influences over the catalytic performance (Fig. 5 and Fig. S3, supplementary information). In general, an increase of the overall ethanol transformation was observed for La-containing catalysts, with an ethanol conversion higher than 70% for all the samples. At the same time, the selectivity to ethylene (the dehydration product from ethanol) increased and it became the main product (Fig. 5A). Apart from the mixed oxide with Mg/La molar ratio of 3, the selectivity of ethylene increased with increasing La content. Accordingly, the ethylene selectivity obtained was 58%, 78% and 87% over the mixed oxide with a Mg/La molar ration of 4, 2 and 1, respectively.

Interestingly, with the presence of La, some ketones, namely acetone and 2-pentanone, were also detected (Fig. 5B). Ketones can be formed through consecutive Tishchenko disproportion reaction [43] of acetaldehyde forming the ester (ethyl acetate, not detected) and consecutive ester ketonization reactions [44], producing water and $CO_2$ as by-products. The reaction mechanism from which ketones can be formed starting from ethanol is depicted in Fig. S4, supplementary information. In particular, the mixed oxide with Mg/La of 3, which led to a slightly lower production of ethylene (52% of ethylene selectivity), led to the highest value of the ketones products, with a total selectivity of 16%.

In comparison, the catalytic activity of pure $La_2O_3$ is lower, in accordance with its low surface area (see Table 1), leading to an ethanol conversion of ca. 29%. It mainly acted as acid catalyst, producing ethylene as main product with a selectivity as high as 73%.

In order to evaluate the effect of the catalytic system composition over the kinetics of the reaction, a reaction with a lower reaction temperature (350 ºC) has been performed with the mixed oxide with a Mg/La molar ratio of 3. The catalytic results are reported in Fig. 6.

By decreasing the reaction temperature from 400 °C to 350 °C while performing the reaction over the mixed oxide with Mg/La= 3 molar ratio, ethanol conversion decreased drastically from 75.4% to 20.2%, as kinetically expected. Ethylene was again the main reaction product and its selectivity increased from 51.9% to 77.6% (Table S3).

In general, at comparable value of ethanol conversion, the presence

**Table 3**
Ethanol conversion and selectivity to the main reaction products obtained over the hydrotalcite-based catalysts and the pure oxides MgO and $La_2O_3$. Reaction conditions: EtOH 5% v/v in $N_2$, T = 400 °C, P = 1 atm, WHSV= 0.3 $g_{ETOH}$ $g_{CAT}^{-1}$ $h^{-1}$).

| Catalyst | Conversion (%) | Selectivity (%) | | | | | | | |
|---|---|---|---|---|---|---|---|---|---|
| | | Acetaldehyde | 1-Butanol | $C_4H_8$[a] | Ethylene | $CO_2$ | Higher Alcohols[b] | Ketones[c] | Others[d] |
| **MgO** | 20 | 31 | 24 | 12 | 16 | 1 | 5 | 4 | 11 |
| **Mg/La= 4** | 74 | 4 | 3 | 7 | 58 | 10 | 0 | 14 | 5 |
| **Mg/La= 3** | 75 | 5 | 4 | 7 | 52 | 10 | 0 | 16 | 5 |
| **Mg/La= 2** | 72 | 2 | 1 | 5 | 78 | 6 | 0 | 4 | 5 |
| **Mg/La= 1** | 84 | 1 | 0 | 5 | 87 | 4 | 0 | 2 | 2 |
| **$La_2O_3$** | 29 | 6 | 1 | 0 | 73 | 4 | 0 | 11 | 6 |

[a] $C_4H_8$: 1,3- butadiene
[b] Higher alcohols: 2-ethyl butanol, 1-hexanol, 2-ethyl butanol
[c] Ketones: acetone, 2-pentanone
[d] Others: ethyl ether, butyraldehyde, ethane

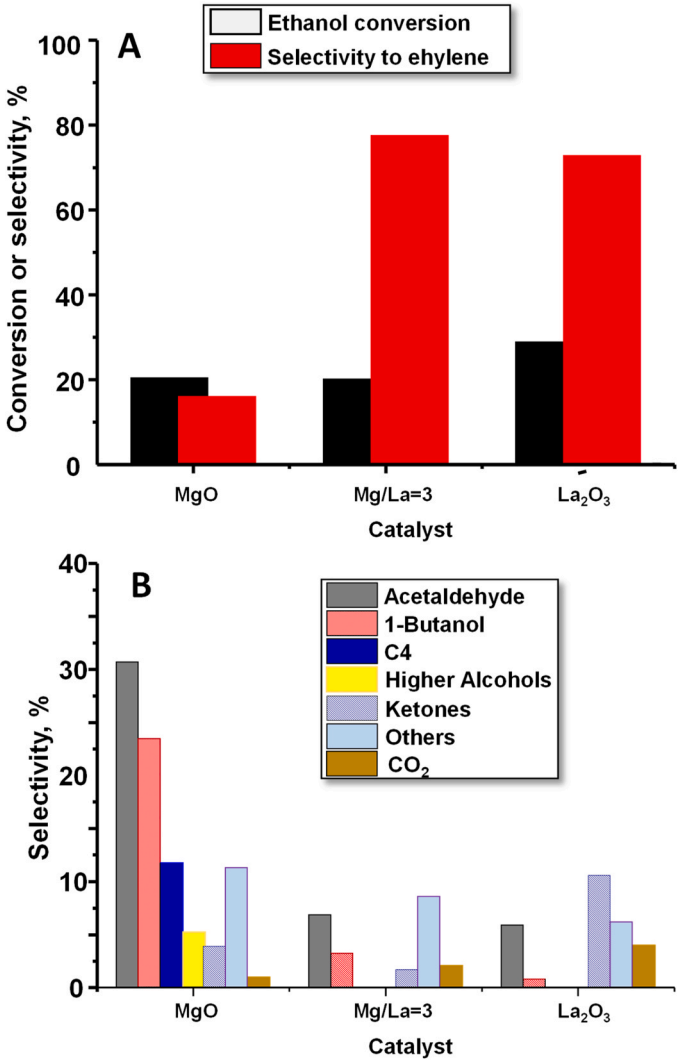


**Fig. 6.** Ethanol conversion and selectivity to ethylene (A) and selectivity to the rest of the reaction products (B) during the ethanol transformation over MgO and $La_2O_3$ at 400 °C and on the mixed-oxide (Mg/La=3 molar ratio) at 350 °C. Reaction conditions: EtOH 5% v/v in $N_2$; P = 1 atm; WHSV= 0.3 $g_{ETOH}$ $g_{CAT}^{-1}h^{-1}$. **Ketones**: acetone, 2-pentanone; **$C_4$**: 1,3-butadiene; **Others**: ethyl ether, butyraldehyde, ethane.

of La led to an increase of catalytic activity carrying acidic properties. Indeed, the dehydration product of ethanol, ethylene, was found to be the main product, a reaction which is acid catalyzed (Fig. S4, supplementary information).

Concerning the catalytic activity, since the mixed Mg/La systems have intermediate surface areas between MgO and $La_2O_3$, the activity of the mixed systems was higher than that of lanthana. However, MgO, shows a lower activity, despite its higher surface area (Table S3). So, it seems that preparing the mixed system is a way to improve the activity with respect to lanthana alone, while substantially keeping the distribution of products of lanthana, even at low La content (Mg/La = 4). In fact, even at low La content, a poor selectivity to acetaldehyde (which instead was very high with MgO), a high selectivity to ethylene (which instead was low with MgO), and a remarkable formation of ketones/$CO_2$ (which is also one feature of $La_2O_3$ and not so much of MgO) was observed.

Overall, it seems that in the mixed systems the behavior is not an average of MgO and $La_2O_3$, but the main features of lanthanum oxide remain the dominant ones, with the further advantage of an improved activity compared to lanthana alone.

### 3.3. Characterization of spent catalysts

Once the catalysts were tested in the ethanol valorization reaction, they were collected and characterized by XRD and XPS.

The study of the used catalysts by XRD, shown in Fig. 2B, reveals an increase of the carbonation of the La-species, in addition to $La(OH)_3$ (PDF number: 00–036–1481), appearing more intense diffractions peaks ascribed to $La_2O_2CO_3$ phase, which is accompanied by a decrease of intensity in the peaks assigned to $La_2O_3$ and/or $La(OH)_3$. Carbonation decreases as the Mg-content in the catalysts increases. Thus, the MgO sample does not show any peak ascribed to the presence of $MgCO_3$. was also observed for spent catalysts.

However, this sample shows the arising of new peaks assigned to the presence of $Mg(OH)_2$ after the reaction, which could be ascribed to the reaction of the produced water during the ethanol condensation with the MgO surface, producing $Mg(OH)_2$. Moreover, the MgO sample shows narrower diffraction peaks after the reactions. This suggests the sintering of the sample along the catalytic process. In addition, the presence of carbonate species could be ascribed to the heterogeneous basic catalysts are prone to suffer strong carbonation on the basic sites.

The surface analysis of the samples after the catalytic tests was also evaluated by XPS are comparatively shown in Fig. 7 (and in Tables S4 and S5, supplementary information). The analysis of C 1 *s* core level spectra of the used catalysts (Fig. 7A) differs in comparison to the fresh catalysts slightly. Thus, it is noteworthy the increase of the contribution ascribed to carbonate species in all cases, which confirms the carbonation of the sample along the reaction and/or the handling of the samples before the XPS experiment. On the other hand, it is also noticeable the arising of a new contribution located about 286.0–286.5 eV, which is assigned to C-OH or C-O-C bonds. This signal could be ascribed to the adsorption between the basic sites with the alcohols. In this sense, previous authors have reported that the alcohols can be deprotonated to form alkoxydes, which interact with the basic sites strongly [45,46].

The study of the O 1 *s* core level spectra of the used catalysts (Fig. 7B) shows a very different profile from that observed for fresh catalysts. Thus, the intensity of the contribution ascribed to oxides species located about 529.0 eV decreases, while the contribution ascribed to carbonate species, about 531.5 eV, increases, confirming the carbonation of the surface of the catalysts. In the same way, it is also noteworthy the arising of a new contribution about 533.0 eV, which is ascribed to the alkoxides strongly joined to the basic sites on the surface of the catalysts.

Regarding to the La $3d_{5/2}$ core level spectra (Fig. 7C), the same contributions reported for fresh catalysts were observed. In the case of Mg 2*p* core level spectra (Fig. 7D), all catalyst display the same contribution ascribed to oxides species, except in the case of MgO catalyst, where a small contribution ascribed to $Mg(OH)_2$ is observed, as was also detected by XRD, which could be due to the presence of water during the dimerization process of ethanol (Guerbet reaction).

The spent catalyst consisting in the Mg:La= 3 molar ratio used after the reaction performed at 400 °C, with a WHSV of 0.3 $g_{ETOH}$ $g_{CAT}^{-1}$ $h^{-1}$) and a total time on stream of 2.6 h was also analyzed by XRD analysis and the corresponding diffractograms included in Fig. 2B. The resulting XRD patterns showed a slight decrease of the overall crystallinity on the spent catalyst, indicating very low changes during the reaction.

## 4. General remarks

A comparison on the characterized through XRD and XPS between fresh and spent catalysts showed the presence of carbonate species, but this was higher over the spent catalyst surfaces, except for the MgO sample. This is the reason why the catalysts were calcined in the same reactor, before the catalytic tests, in order not to favor the formation of carbonates after calcination, which would modify the catalytic properties of these materials.

During the catalyst tests, the formation of $CO_2$ has been observed, which is related to the ketonization reaction (as showed in the reaction

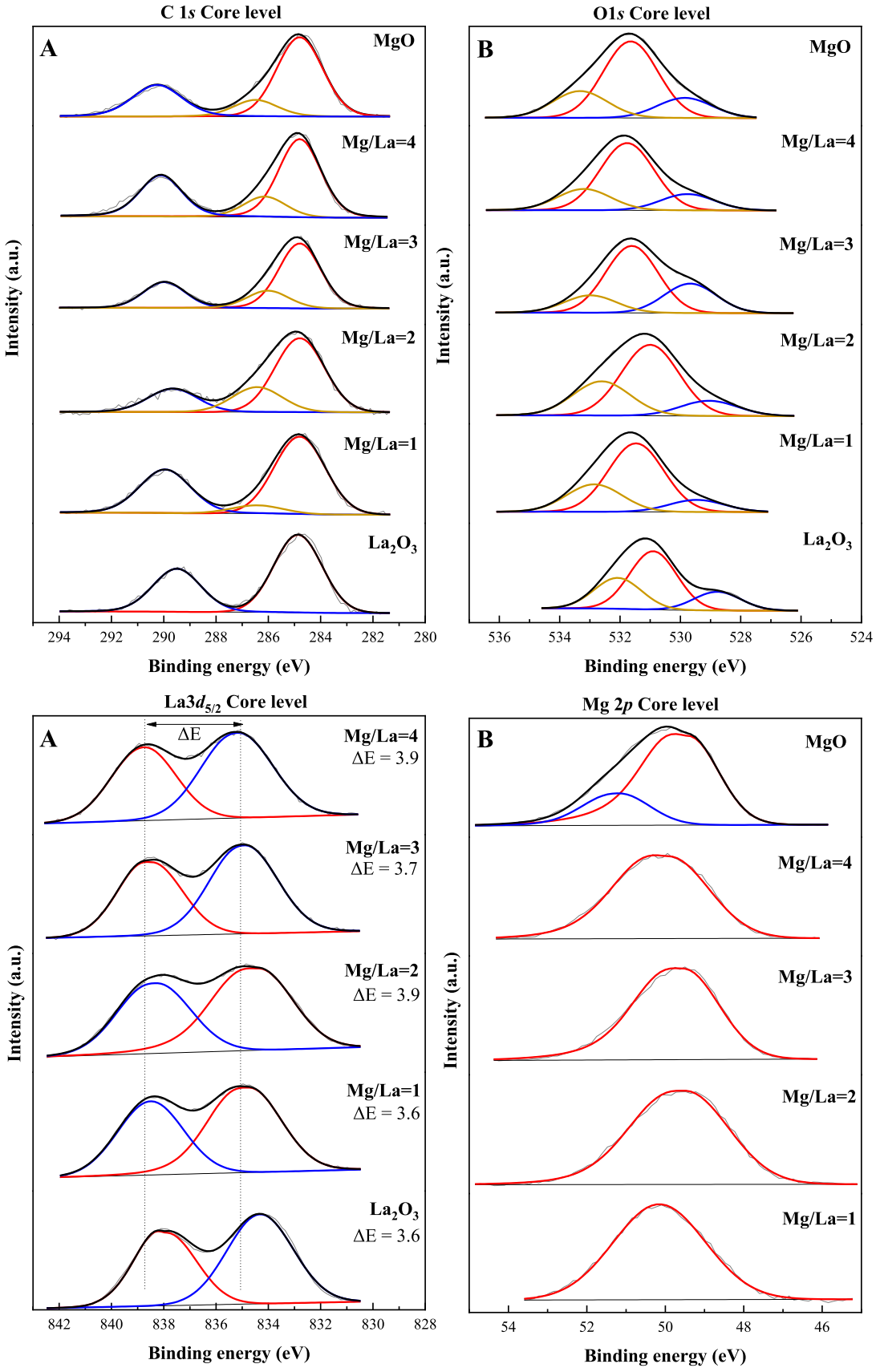


**Fig. 7.** : C 1*s* (A), O 1*s* (B), La $3d_{5/2}$ (C) and Mg 2*p* (D) core level spectra of spent samples.

scheme in Fig. S4). Therefore, the $CO_2$ formation during the reaction can be related to the carbonation of the catalytic surface of the spent catalysts, forming the $La_2O_2CO_3$ phase. On the other hand, the formation of the magnesium hydroxide in the spent MgO sample or $La(OH)_3$ in La-containing catalysts, the presence of which has been observed through XRD analysis (see Fig. 1B) and XPS analysis (see Fig. 7) can be associated to the reaction of the produced water during ethanol condensation with the MgO surface, producing $Mg(OH)_2$ but also $La(OH)_3$.

On the other hand, and according to Fig. S4, the role of acid and basic sites on each reaction step must be highlighted. The main product observed over the catalytic system has been ethylene over all the systems except for the MgO catalyst. The addition of La into the catalysts led to the formation of the acidic sites (as measured through $NH_3$-TPD analysis, see Table 1) responsible for the dehydration of ethanol toward ethylene. For this reason, the higher ethanol conversion should be related to the combination of the two different reaction pathways, as indicated in Fig. S4, as well as the enhanced specific surface area of the mixed-oxide catalysts, as determined through BET analysis (see Table 1).

## 5. Conclusions

MgO-$La_2O_3$ catalysts with different Mg/La molar ratio were synthesized by a precipitation method and subsequent calcination, obtaining catalysts where both $La_2O_3$ and MgO are highly dispersed. These catalysts present basicity although their acidity and textural properties were relatively low.

Considering the availability of the basic sites, MgO-$La_2O_3$ catalysts were tested in the selective transformation of ethanol into valuable products. MgO-catalyst, which displayed higher basicity and traditionally used in the Guerbet reaction, showed the poorest activity and led to the formation of n-butanol as the main product and acetaldehyde. The incorporation of lanthanum promotes the formation of small amount of acid sites. The modification of the acid-bases properties influences in the catalytic performance improving the ethanol conversion, reaching values above 70% in all La-based catalysts. Regarding to the selectivity pattern, the presence of lanthanum promotes the dehydration of ethanol, obtaining ethylene as main product. In particular, the maximum ethylene selectivity is attained for the Mg/La catalyst with a molar ratio of 1 (i.e., 87%).

## CRediT authorship contribution statement

**D. Ballesteros Plata**: Methodology, Investigation, Data curation, Writing – review. **G. Balestra**: Methodology, Investigation, Data curation, Writing – review. **J. A. Cecilia:** Methodology, Data curation, Writing – review & editing. **I. Barroso Martín**: Investigation, Data curation. **A. Infantes-Molina**: Methodology, Data curation, Writing – review & editing. **T. Tabanelli:** Data curation, Writing – review & editing. **F. Cavani:** Conceptualization, Writing – review & editing, Supervision. **M. Montaña:** Investigation, Data curation. **J.M. López Nieto:** Conceptualization, Resources, Data curation, Writing – review & editing, Supervision. **E. Rodríguez Castellón**: Conceptualization, Resources, Data curation, Writing – review & editing, Supervision.

## Declaration of Competing Interest

The authors declare that they have no known competing financial interests or personal relationships that could have appeared to influence the work reported in this paper.

## Data availability

Data will be made available on request.

## Acknowledgements

The funding received for this study from the Spanish Ministry of Science and Innovation, PID2021–126235OB-C31 and PID2021–126235OB-C32 funded by MCIN/ AEI/10.13039/ 501100011033 and FEDER funds, and projects TED2021–130756B-C31 and TED2021–130756B-C32 funded by MCIN/AEI/10.13039/ 501100011033 and by "ERDF A way of making Europe" by the European Union NextGenerationEU/PRTR, is acknowledged.

## Appendix A. Supporting information

Supplementary data associated with this article can be found in the online version at doi:10.1016/j.cattod.2023.114470.

## References

[1] A. Corma, S. Iborra, A. Velty, Chemical routes for the transformation of biomass into chemicals, Chem. Rev. 107 (2007) 2411–2502.
[2] M.C.P. Gonçalves, J.P. Romanelli, A.B.M. Cansian, E.F.Q. Pucci, J.R. Guimarães, P. W. Tardioli, B.A. Saville, A review on the production and recovery of sugars from lignocellulosics for use in the synthesis of bioproducts, Ind. Crops Prod. 186 (2022), 115213.
[3] Global Ethanol Production by Country or Region. Available online: ⟨https://afdc.energy.gov/data/10331/⟩.
[4] T.D. Houng, N. Nghiem, Recent developments and current status of commercial production of fuel ethanol, Fermentation 7 (2021) 314.
[5] R.P. John, G.S. Anisha, K.M. Nampoothiri, A. Pandey, Micro and macroalgal biomass: a renewable source for bioethanol, Bioresour. Technol. 102 (2011) 186–193.
[6] V. Menon, M. Rao, Trends in bioconversion of lignocellulose: biofuels, platform chemicals & biorefinery concept, Prog. Energ. Combust. 38 (2012) 522–550.
[7] B.G. Harvey, H.A. Meylemans, The role of butanol in the development of sustainable fuel technologies, Chem. Technol. Biotechnol. 86 (2011) 2–9.
[8] M. Ghanta, D. Fahey, B. Subramaniam, Environmental impacts of ethylene production from diverse feedstocks and energy sources, Appl. Pet. Res 4 (2014) 167–179.
[9] S. Najari, S. Saeidi, P. Concepcion, D.D. Dionysiou, S.K. Bhargava, A.F. Lee, K. Wilson, Oxidative dehydrogenation of ethane: catalytic and mechanistic aspects and future trends, Chem. Soc. Rev. 50 (2021) 4564–4605.
[10] M.C.H. Clemente, G.A.V. Martins, E.F. de Freitas, J.A. Días, S.C.L. Días, Ethylene production via catalytic ethanol dehydration by 12-tungstophosphoric acid@ceria-zirconia, Fuel 239 (2019) 491–501.
[11] J.C. Soh, S.L. Chong, S.S. Hossain, C.K. Cheng, Catalytic ethylene production from ethanol dehydration over non-modified and phosphoric acid modified Zeolite H-Y (80) catalysts, Fuel Process. Technol. 158 (2017) 85–95.
[12] H. Zhu, A. Ramanathan, J.F. Wu, B. Subramaniam, Genesis of strong Brønsted acid sites in WZr-KIT-6 catalysts and enhancement of ethanol dehydration activity, ACS Catal. 8 (2018) 4848–4859.
[13] D. Fan, D.J. Dai, H.S. Wu, Ethylene formation by catalytic dehydration of ethanol with industrial considerations, Materials 6 (2013) 101–115.
[14] Z. Wang, L.A. O'Dell, X. Zeng, C. Liu, S. Zhao, W. Zhang, M. Gaborieau, Y. Jiang, J. Huang, Insight into three-coordinate aluminum species on ethanol-to-olefin conversion over ZSM-5 zeolites, Angew. Chem. Int. Ed. 58 (2019) 18061–18068.
[15] G. Chen, S. Li, F. Jiao, Q. Yuan, Catalytic dehydration of bioethanol to ethylene over $TiO_2/\gamma$-$Al_2O_3$ catalysts in microchannel reactors, Catal. Today 125 (2007) 111–119.
[16] Y. Chen, Y. Wu, L. Tao, B. Dai, M. Yang, Z. Chen, X. Zhu, Dehydration reaction of bio-ethanol to ethylene over modified SAPO catalysts, J. Ind. Eng. Chem. 16 (2010) 717–722.
[17] A. Galadima, O. Muraza, Zeolite catalysts in upgrading of bioethanol to fuels range hydrocarbons: a review, J. Ind. Eng. Chem. 31 (2015) 1–14.
[18] T.K. Phung, A. Lagazzo, M.Á. Rivero Crespo, V. Sánchez Escribano, G. Busca, A study of commercial transition aluminas and of their catalytic activity in the dehydration of ethanol, J. Catal. 311 (2014) 102–113.
[19] H. Chiang, A. Bhan, Catalytic consequences of hydroxyl group location on the rate and mechanism of parallel dehydration reactions of ethanol over acidic zeolites, J. Catal. 271 (2010) 251–261.
[20] H. Xin, X. Li, Y. Fang, X. Yi, W. Hu, Y. Chu, F. Zhang, A. Zheng, H. Zhang, X. Li, Catalytic dehydration of ethanol over post-treated ZSM-5 zeolites, J. Catal. 312 (2014) 204–215.
[21] Y. Furumoto, Y. Harada, N. Tsunoji, A. Takahashi, T. Fujitani, Y. Ide, M. Sadakane, T. Sane, Effect of acidity of ZSM-5 zeolite on conversion of ethanol to propylene, Appl. Catal. A: Gen. 399 (2011) 262–267.
[22] J. Li, Z. Wei, Y. Chen, B. Jing, Y. He, M. Dong, H. Jiao, X. Li, Z. Qin, J. Wang, W. Fan, A route to form initial hydrocarbon pool species in methanol conversion to olefins over zeolites, J. Catal. 317 (2014) 277–283.
[23] D. Varisli, T. Dogu, G. Dogu, Ethylene and diethyl-ether production by dehydration reaction of ethanol over different heteropolyacid catalysts, Chem. Eng. Sci. 62 (2007) 5349–5352.

[24] U. Filek, A. Kirpsza, A. Micek-Ilnicka, E. Lalik, A. Bielański, Ethanol conversion over cesium-doped mono- and bi-cationic aluminum and gallium $H_3PW_{12}O_{40}$ salts, J. Mol. Catal. A-Chem. 407 (2015) 152–162.
[25] A. Mohsenzadeh, A. Zamani, M.J. Taherzadeh, Bioethylene production from ethanol: a review and techno-economical evaluation, ChemBioEng. Rev. 4 (2017) 75–91.
[26] S. Karimi, M. Tavakkoli Yaraki, R. Rao Karri, A comprehensive review of the adsorption mechanisms and factors influencing the adsorption process from the perspective of bioethanol dehydration, Renew. Sustain. Energy Rev. 107 (2019) 535–553.
[27] A. Chieregato, J. Velasquez, Ochoa, C. Bandinelli, G. Fornasari, F. Cavani, M. Mella, On the chemistry of ethanol on basic oxides: revising mechanisms and intermediates in the Lebedev and Guerbet reactions, ChemSusChem 8 (2015) 377–388.
[28] C. Angelici, M.E.Z. Velthoen, B.M. Weckhuysen, P.C.A. Bruijnincx, Influence of acid–base properties on the Lebedev ethanol-to-butadiene process catalyzed by $SiO_2$-MgO materials, Catal. Sci. Technol. 5 (2015) 2869–2879.
[29] C. Cesari, A. Gagliardi, A. Messori, N. Monti, V. Zanotti, S. Zacchini, I. Rivalta, F. Calcagno, C. Lucarelli, T. Tabanelli, F. Cavani, R. Mazzoni, Boosting the guerbet reaction: A cooperative catalytic system for the efficient bio-ethanol refinery to second-generation biofuels, J. Catal. 405 (2022) 47–59.
[30] G. Garbarino, R.P. Parameswari Vijayakumar, P. Riani, E. Finocchio, G. Busca, Ethanol and diethyl ether catalytic conversion over commercial alumina and lanthanum-doped alumina: Reaction paths, catalyst structure and coking, Appl. Catal. B: Envion 236 (2018) 490–500.
[31] S. Kang, D. Lee, S. Kwon, Lanthanum doping for longevity of alumina catalyst bed in hydrogen peroxide thruster, Aerosp. Sci. Technol. 46 (2015) 197–203.
[32] P. Alphonse, B. Faure, Thermal stabilization of alumina modified by lanthanum, Micropor. Mesopor. Mat. 196 (2014) 191–198.
[33] N. Zhan, Y. Hu, H. Li, D. Yu, Y. Han, H. Huang, Lanthanum–phosphorous modified HZSM-5 catalysts in dehydration of ethanol to ethylene: a comparative analysis, Catal. Commun. 11 (2010) 633–637.
[34] M. Weihe, M. Hunger, M. Breuninger, H.G. Karge, J. Weitkamp, Influence of the nature of residual alkali cations on the catalytic activity of zeolites X, Y, and EMT in their Brønsted acid forms, J. Catal. 198 (2001) 256–265.
[35] J. Ouyang, F. Kong, G. Su, Y. Hu, Q. Song, Catalytic conversion of bio-ethanol to ethylene over La-modified HZSM-5 catalysts in a bioreactor, Catal. Lett. 132 (2009) 64–74.
[36] A. Corma, J.M. López Nieto, N. Paredes, Influence of the preparation methods of V-Mg-O catalysts on their catalytic properties for the oxidative dehydrogenation of propane, J. Catal. 144 (1993) 425–438.
[37] M. Thommes, K. Kaneko, A.V. Neimark, J.P. Oliver, F. Rodríguez-Reinoso, J. Rouquerol, K.S.W. Sing, Physisorption of gases, with special reference to the evaluation of surface area and pore size distribution (IUPAC Technical Report), Pure Appl. Chem. 87 (2015) 1051–1069.
[38] S. Brunauer, P.H. Emmett, E. Teller, Adsorption of gases in multimolecular layers, J. Am. Chem. Soc. 60 (1938) 309–319.
[39] J.F. Moulder, W.F. Stickle, P.E. Sobol, K.D. Bomben, Handbook of X-Ray Photoelectron Spectroscopy, Perkin-Elmer Corporation, Physical Electronics Division, Eden Prairie, Minnesota, USA, 1992.
[40] W. Ueda, T. Kuwabara, T. Ohshida, Y. Morikawa, A low-pressure Guerbet reaction over magnesium oxide catalyst, J. Chem. Soc., Chem. Commun. (1990) 1558–1559.
[41] A.C. Dimian, C.S. Bildea, Novel one-stage process for manufacturing 1,3-butadiene from ethanol, Chem. Eng. Res. Des. 193 (2023) 460–478.
[42] W.E. Taifan, T. Bučko, J. Baltrusaitis, Catalytic conversion of ethanol to 1,3-butadiene on MgO: a comprehensive mechanism elucidation using DFT calculations, J. Catal. 346 (2017) 78–91.
[43] M. Kayanuma, Y. Shinke, T. Miyazawa, T. Fujitani, Y.-K. Choe, Understanding composition-dependent catalytic performance of PdAg for the hydrogenation of 1,3-butadiene to 1-butene, Catal. Commun. 149 (2021), 106239.
[44] E. Jamalzade, K. Kashkooli, L. Griffin, L, G.P. van Walsum, T.J. Schwartz, Production of jet-fuel-range molecules from biomass-derived mixed acids, React. Chem. Eng. 6 (2021) 845–857.
[45] M.S. Gyngazova, L. Grazia, A. Lolli, G. Innocenti, T. Tabanelli, M. Mella, S. Albonetti, F. Cavani, Mechanistic insights into the catalytic transfer hydrogenation of furfural with methanol and alkaline earth oxides, J. Catal. 372 (2019) 61–73.
[46] R. López-Asensio, J.A. Cecilia-Buenestado, C. Herrera-Delgado, M.A. Larrubia-Vargas, C. García-Sancho, P.J. Maireles-Torres, R. Moreno-Tost, Mixed oxides derived from hydrotalcites Mg/Al active in the catalytic transfer hydrogenation of furfural to furfuryl alcohol, Catalysts 13 (2023) 45.